Magnetic and structural properties of nickel zinc ferrite nanoparticles synthesized at room temperature

Shannon A. Morrison
The George Washington University, Washington, D.C. 20052 and U.S. Naval Research Laboratory, Washington, D.C. 20375

Christopher L. Cahill
The George Washington University, Washington, D.C. 20052

Everett E. Carpenter[a)]
U.S. Naval Research Laboratory, Washington, D.C. 20375

Scott Calvin
Sarah Lawrence College, Bronxville, New York 10708

Raja Swaminathan and Michael E. McHenry
Carnegie Mellon University, Pittsburgh, Pennsylvania 15213

Vincent G. Harris
Northeastern University, Boston, Massachusetts 02115

Nickel zinc ferrite nanoparticles ($Ni_{0.20}Zn_{0.44}Fe_{2.36}O_4$) have been produced at room temperature, without calcination, using a reverse micelle process. Particle size is approximately 7 nm as determined by x-ray powder diffraction and transmission electron microscopy. Saturation magnetization values are lower than anticipated, but are explained by elemental analysis, particle size, and cation occupancy within the spinel lattice. Extended x-ray absorption fine structure analysis suggests that a significant amount of Zn^{2+}, which normally occupies tetrahedral sites, actually resides in octahedral coordination in a zinc-enriched outer layer of the particles. This "excess" of diamagnetic Zn can thus contribute to the overall decrease in magnetism. Further, this model can also be used to suggest a formation mechanism in which Zn^{2+} is incorporated at a later stage in the particle growth process. © *2004 American Institute of Physics.*
[DOI: 10.1063/1.1715132]

I. INTRODUCTION

Nickel zinc ferrite (NZFO) has found use in electromagnetic applications that require a high permeability, such as inductors and electromagnetic wave absorbers.[1] Current interest has been to make nanosized NZFO particles in order to reduce energy losses associated with bulk powders. Further, most electronic applications require these materials be pressed into larger shapes with near theoretical density, which is difficult to obtain if the particles have a wide size distribution. Though several methods of nanoscale ferrite synthesis have been successful in making NZFO, such as hydrothermal,[2–5] coprecipitation,[6–9] and ball milling,[10] control of the particle size and distribution has remained elusive.

Reverse micelle synthesis is a technique that has demonstrated considerable control over nanoparticle size and distribution in other oxide systems.[11–13] Briefly, reverse micelles are water-in-oil emulsions in which the water to surfactant ratio controls the size of water pools within which aqueous chemical syntheses take place, and consequently control the size of resultant particles.[14] This technique is particularly attractive for room temperature reactions such as the precipitation of oxide nanoparticles.[15] Synthesis of various nanoparticles within reverse micelles, specifically ferrites, has demonstrated the ability to control the particle size, size distribution,[13,16] chemical stoichiometry, and cation occupancy.[17] However, previous work has often produced "precursor" particles that require subsequent firing.[8,18]

Our recent efforts have focused on the room-temperature synthesis of nanoscale NZFO ferrites that do not require further processing. In the study presented herein, we have employed a surfactant system for the room-temperature reverse micelle synthesis of NZFO nanoparticles. Sodium dioctylsulfosuccinate (AOT),[19,20] was combined with a 2,2,4-trimethylpentane (isooctane) oil phase to make the reverse micelle solution. This allowed comparison to similarly produced materials from other research groups in which NZFO was synthesized in reverse micelles and subsequently *fired* to produce the desired product; our material did not need a subsequent firing step. We have optimized the reaction conditions of this system to produce, at room temperature, pure phase nanoscale NZFO particles over a narrow size distribution. This paper outlines the synthetic route in the AOT system and examines the magnetic behavior and cation distribution within this ferrite structure.

II. EXPERIMENT

For the AOT/isooctane reverse micelle system, a stock solution of 0.5M AOT was prepared in isooctane. An aque-
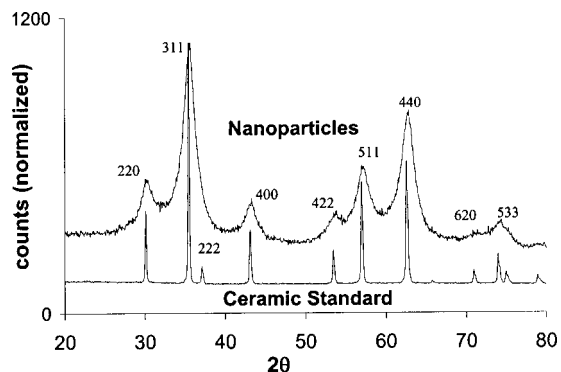
---

a)Email address: carpenter@anvil.nrl.navy.mil

J. Appl. Phys., Vol. 95, No. 11, 1 June 2004

Morrison *et al.* 6393

FIG. 1. X-ray powder diffraction of NZFO nanoparticles and a ceramic bulk sample.

FIG. 2. TEM of NZFO nanoparticles.

ous metal solution was then prepared using 0.045M FeCl$_2$, 0.011M NiCl$_2$, and 0.011M ZnCl$_2$. The AOT solution was added volumetrically to the aqueous metal solution to form a reverse micelle solution. An analogous solution was made using water and concentrated ammonia in a 1:1 ratio. The ammonia solution was used to adjust the pH of the aqueous metal solution to induce precipitation and oxidation within the water pools. The mole ratio of ammonia to metal cations was greater than 12:1 and the relative volume of AOT solution to water was 6:1, corresponding to an ω of 16.5.

Both the metal containing reverse micelle solution and the corresponding ammonia solution were agitated until each was visibly clear, sonicated for 5 min and then purged with flowing nitrogen for 5 min. The metal solution was placed in an addition funnel and added to the ammonia solution while stirring. Once the addition was complete, the reaction was stirred for 2 h. Excess methanol was added and mixed with the reverse micelle solution to disrupt the micelles and remove surfactant from the particles. This mixture was centrifuged and the supernatant removed. The material was washed and centrifuged repeatedly ($\sim 10 \times$) with methanol and then methanol/water until the AOT was removed. The material was then dried over-night in a vacuum chamber.

X-ray powder diffraction was performed on the NZFO particles using a Phillips x-ray diffractometer employing Cu $K\alpha$ radiation from a sealed tube (50 kV, 30 mA) source. Analysis of the material revealed a match with PDF # 08-0234,[21] indicating the nickel zinc ferrite structure (Fig. 1). Using the Scherrer equation, a crystallite diameter of 6.8 nm was determined.

A TECNAI F20 model high-resolution transmission electron microscope (TEM) was used to characterize the morphologies and the particle size distribution of the nanoparticles (Fig. 2). The NZFO nanoparticles were suspended in methanol and agitated in an ultrasonic bath. The TEM sample was prepared by placing a few drops of this suspension on a holey C film. The particle size distribution was estimated based on analyzing the bright field images of randomly selected nanoparticles. The average particle size was estimated to be 6.2 nm.

The elemental composition of the sample was determined using a PE Optima 4000 inductively coupled plasma–Optical Emission Spectrometer (ICP-OES). Samples for ICP-OES were prepared by dissolving in concentrated nitric acid in an acid digestion bomb at 170 °C. Analysis of the data yielded the following molar percentages of metal composition: Ni:Zn:Fe 6.4:14.8:78.8. Magnetic properties were measured using a Quantum Design MPMS-5S SQUID magnetometer. Evaluation of the hysteresis loop (Fig. 3) gives a saturation magnetization of 25.9 emu/g at 300 K and 38.5 emu/g at 10 K, with coercivities of 16 and 63 Oe, respectively.

Extended x-ray absorption fine structure (EXAFS) spectra were collected at the National Synchrotron Light Source at Brookhaven National Laboratory using the NRL consortium beam lines X23B and X11A. A detailed description of the data collection methods and the analytical methodology can be found in Calvin *et al.*[22] EXAFS indicated that the material is single-phase spinel (Table I), in agreement with the XRD results. Preliminary EXAFS analysis suggested that the particles are not homogeneous with respect to chemical composition. A better fit to the data is achieved using a two-layer model (Fig. 4) in which the Zn metal ions have a greater concentration in the outer layer as compared to the center of the nanoparticles. The two-layer model yields (39 $\pm$ 19)% of the zinc cations in octahedral sites (Table I), which contradicts the usual expectation of zinc occupying only tetrahedral sites. Both the homogeneous and two-layer models indicate that nickel cations occupy predominately octahedral sites.

III. DISCUSSION

As can be seen from the magnetization versus temperature plot (Fig. 3(b), insert), the particles are superparamagnetic above a blocking temperature of 50 K. A saturation magnetization of 25.9 emu/g was measured at 300 K, well above the blocking temperature, and was less than half the value of 70.3 emu/g for a ceramic standard. This value was also low when compared to published values for other nano-
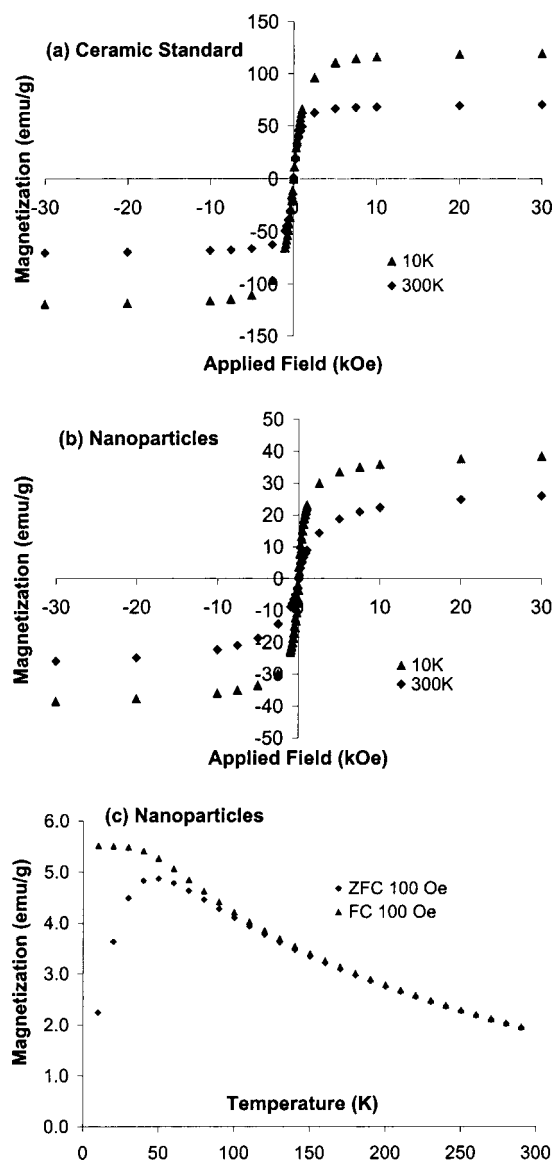
FIG. 3. (a) Hysteresis loop for NZFO bulk ceramic standard (b) and NZFO nanoparticles, measured at (▲) 10 K and (◆) 300 K. (c) Magnetization vs temperature plot for the nanoparticles.
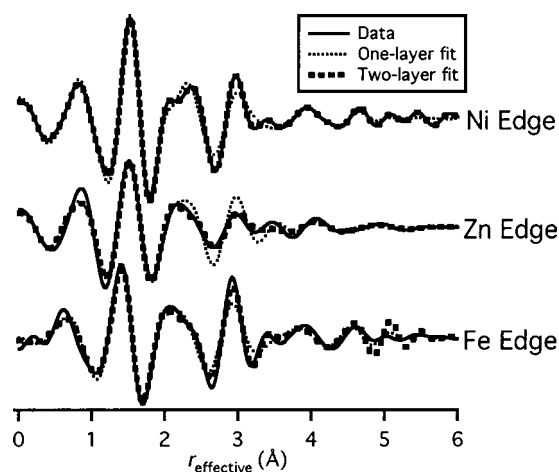

FIG. 4. Real part of the EXAFS Fourier transforms for the three metallic constituents. Fits using the one-layer and two-layer models are also shown.

Whereas size effects could explain the reduced magnetic saturation at room temperature, at temperatures below the blocking temperature the reduction can be further attributed to both elemental composition and site occupancies of the metal cations in the oxygen lattice. The NZFO ferrite presented herein, as verified by XRD and EXAFS, has the spinel crystal structure, and therefore consists of a face-centered-cubic array of oxygen atoms with cations occupying 1/8 of the tetrahedral sites and 1/2 of the octahedral sites. In order to balance the overall charge in this system, there is one cation in a $+2$ oxidation state and two cations in a $+3$ oxidation state for every four oxygen atoms. Since Zn and Ni prefer the $+2$ oxidation state, all of the $+3$ ions are therefore Fe. The ideal NZFO ferrite has the molar ratio $Ni_{1-x}Zn_xFe_2O_4$; ICP results for our material, normalized to the ferrite notation are 0.19:0.44:2.36, indicating that some zinc and over half the nickel was lost in the synthesis. The ratio of Fe to Zn and Ni combined is more than 2:1, and EXAFS does not indicate any cation vacancies, thus requiring that some of the iron adopt the $+2$ oxidation state as well. Support for this conclusion can be found in the higher mean square radial displacement value for Fe (Table I) compared to Ni and Zn, suggesting that the Fe occupies more than one oxidation state within the material. Research into similar ferrite systems indicates that Fe^{+2} preferentially occupies octahedral sites. Since the overall saturation magnetization is a combination of the spin only moments in the octahedral lattice minus the spin only moments in the tetrahedral lattice, reduction of Fe^{+3} to Fe^{+2} would lower the overall saturation magnetization.

In the inverse spinel structure, such as nickel zinc ferrites, nickel normally occupies an octahedral site, whereas the zinc occupies tetrahedral sites. EXAFS analysis for these samples suggest that the zinc is not evenly distributed within the individual particles giving the Ni:Zn:Fe molar ratio as 0.01:0.27:0.71 in the tetrahedral sites, and 0.09:0.09:0.82 in the octahedral sites. Though zinc occupancy of the octahedral site is not unprecedented,[23] this is considered an indication of substantial cation disorder. Overloading of the outer layers by the zinc cations is proposed as the reason zinc

scale NZFO particles. A value of 44 emu/g at room temperature was reported for a coprecipitated particle 50 nm in diameter with a 16 nm crystallite, heated at 80 °C for 36 h.[8] This lower value is consistent with particle size effects on saturation magnetization. Likewise, the saturation magnetization when measured at 10 K was lower, with a value of 38.5 emu/g for the nanoparticles, as compared to 119 emu/g for the ceramic sample.

TABLE I. Results determined from EXAFS fit using a two-layer model.

	Ni	Zn	Fe
Lattice parameter (Å)	8.49(4)		
Oxygen parameter	0.387(8)		
EXAFS r factors	0.031	0.032	0.033
Percent of cation in octahedral sites	95	39(19)	
MSRD (metal-O nearest neighbor) (Å^2)	0.004(4)	0.006(5)	0.011(4)

occupies some of the octahedral sites. As a result of the zinc cation being diamagnetic, it cannot participate in superexchange coupling between the octahedral and tetrahedral lattices; therefore an inhomogeneous excess of zinc in the ferrite would disrupt some magnetic coupling and lead to an overall reduction in magnetism.

It is still unclear as to why this reverse micelle system has allowed formation of ferrite nanoparticles at room temperature, when other similar syntheses have required annealing.[8,18] We speculate that an important factor in the synthesis is the pH range of the micelle solution. Metal cations in the micelle water pools will convert to their hydroxide form *en route* to the formation of the ferrite. For each species, the conversion of the metal ions to the hydroxide and then oxide form is controlled primarily by the pH. Since Zn^{2+} remains soluble over a wider pH range than the other cations,[24] it may precipitate at a later stage onto a nickel ferrite "nucleus," In a fashion consistent with the two-layer compositional model suggested by EXAFS. In reality, there is most likely a complex interplay of several factors, including the buffering capacity of AOT,[25] the solubility of the cations across a range of pH, oxidation rates, and other surfactant related influences on particle growth. A more detailed examination of these phenomena and efforts to homogenize cation concentrations in the particles are ongoing and will be the subject of a forthcoming paper.

IV. CONCLUSION

Single-phase nanosized NZFO particles were successfully prepared using a room-temperature reverse micelle process without requiring subsequent firing of the material. Individual particles however, show a nonequilibrium distribution of cations throughout their expected lattice sites, leading to a reduction in saturation magnetization. EXAFS analysis of this inhomogeneity suggests a two-layer model for the distribution of Zn^{2+} cations within the nanoparticles. It is plausible that this inhomogeneity exists in "as-synthesized" particles in other systems and that annealing may redistribute the cations into a more homogeneous product. Evidence for this can be inferred from Kumar *et al.*[8] who do not report a detailed chemical or structural analysis, but do observe an increase in saturation magnetization of NZFO nanoparticles with increasing calcination. Though the particle size influences the physical properties of the material, investigation into its effect has not been pursued as deviation from ideal ferrite metal ratios ($Ni_{1-x}Zn_xFe_2O_4$) and the aforementioned concentration gradient likely cloud this effect. However, we have developed considerable insight into the atomic composition of the material with a desire to understand the effects upon the subsequent physical proper-

ties. Further work is underway to investigate the removal of cation concentration gradients through both the modification of synthetic parameters as well as post processing annealing. The effect of particle size on the physical properties will also be the focus of future work.

[1] T. Tsutaoka, J. Appl. Phys. **93**, 2789 (2003).
[2] A. Dias and V. T. L. Buono, J. Mater. Res. **12**, 3278 (1997).
[3] A. Cabanas and M. Poliakoff, J. Mater. Chem. **11**, 1408 (2001).
[4] Y. Tamura, T. Sasao, M. Abe, and T. Itoh, J. Colloid Interface Sci. **136**, 242 (1990).
[5] A. Dias and R. L. Moreira, Mater. Lett. **39**, 69 (1999).
[6] H. J. Song, J. H. Oh, S. C. Choi, and J. C. Lee, Phys. Status Solidi A **189**, 849 (2002).
[7] P. C. Fannin, S. W. Charles, and J. L. Dormann, J. Magn. Magn. Mater. **201**, 98 (1999).
[8] P. S. A. Kumar, J. J. Shrotri, S. D. Kulkarni, C. E. Deshpande, and S. K. Date, Mater. Lett. **27**, 293 (1996).
[9] A. S. Albuquerque, J. D. Ardisson, W. A. A. Macedo, and M. C. M. Alves, J. Appl. Phys. **87**, 4352 (2000).
[10] J. S. Jiang, L. Gao, X. L. Yang, J. K. Guo, and H. L. Shen, J. Mater. Sci. Lett. **18**, 1781 (1999).
[11] M. P. Pileni, Cryst. Res. Technol. **33**, 1155 (1998).
[12] J. Sims, A. Kumbhar, J. Lin, F. Agnoli, E. Carpenter, C. Sangregorio, C. Frommen, V. Kolesnichenko, and C. J. O'Connor, Mol. Cryst. Liq. Cryst. **379**, 113 (2002).
[13] C. J. O'Connor, C. T. Seip, E. E. Carpenter, S. C. Li, and V. T. John, Nanostruct. Mater. **12**, 65 (1999).
[14] J. Rivas, M. L. Quintela, J. L. Perez, and L. Liz, IEEE Trans. Magn. **29**, 2655 (1993).
[15] M. Lade, H. Mays, J. Schmidt, R. Willumeit, and R. Schomacker, Colloids Surf., A **163**, 3 (2000).
[16] M. P. Pileni, A. Hammouda, N. Moumen, and I. Lisiecki, in *Fine Particle Science and Technology*, edited by E. Pelizzetti (Kluwer Academic, Netherlands, 1996), p. 413–429.
[17] E. E. Carpenter, C. J. O'Connor, and V. G. Harris, J. Appl. Phys. **85**, 5184 (1999).
[18] D. O. Yener and H. Giesche, J. Am. Ceram. Soc. **84**, 1987–1995 (2001).
[19] C. T. Seip, E. E. Carpenter, C. J. O'Connor, V. T. John, and S. Li, IEEE Trans. Magn. **34**, 1111 (1998).
[20] K. Lee, C. Sorenson, K. Klabunde, and G. Hadjipanayis, IEEE Trans. Magn. **28**, 3180 (1992).
[21] K. Kedesky, *PDF Card Reference* (International Centre for Diffraction Data, Newtown Square, PA, 1996).
[22] S. Calvin, E. E. Carpenter, B. Ravel, V. G. Harris, and S. A. Morrison, Phys. Rev. B **66**, 224405.1 (2002).
[23] S. A. Oliver, V. G. Harris, H. H. Hamdeh, and J. C. Ho, Appl. Phys. Lett. **76**, 2761 (2000).
[24] M. Pourbaix, *Atlas of Electrochemical Equilibria in Aqueous Solutions* (NACE International, Cebelcor, 1974).
[25] M. Hasegawa, Langmuir **17**, 1426 (2001).